Electronic Supplementary Material (ESI) for Chemical Communications.

Supporting Information

Enhanced electron transfer by In doping in SnO_2 for efficient CO_2 electroreduction to C_1 products

Chemicals:

All reagents were of analytical grade and used without further purification. The Indium chloride ($InCI_3$) and sodium stannate trihydrate (Na_2SnO_3) were purchased from Macklin Biochemical Co., Ltd. The ethanol (C_2H_5OH), potassium bicarbonate ($KHCO_3$), potassium hydroxide (KOH), ethnanolamine (C_2H_7NO) and dimethyl sulfoxide (DMSO) were purchased from Sinopharm Chemical Reagent Co., Ltd. The Nafion 211 membrane, bipolar membrane, carbon paper, gas diffusion layer, carbon rods and glassy carbon electrode were purchased from Gaoss Union Technology Co., Ltd. The PH test papers (1-14) and nickel foam were bought from Taobao. All the deionized water (18.25 kΩ) used for solution preparation and instrument cleaning was homemade by UPT-II-10T ultrapure water system.

Synthesis:

To prepare In-SnO_2-1/1, 1 mmol $InCI_3$, 1 mmol Na_2SnO_3 were first uniformly dispersed in 25 mL ultrapure water to form a white suspension. Then, 5 M NaOH was added drop by drop to the above solution and vigorously stirred more than 30 min. Subsequently, the fully dissolved transparent solution was transferred into a 50 mL Teflon-lined autoclave and kept at 180°C for 24 h in an oven. After washed with ethanol and deionized water alternately for three times, the obtained white precipitate was dried in a vacuum oven at 60°C. For comparison, the In-SnO_2-0/1, In-SnO_2-0.5/1, In-SnO_2-2/1, In-SnO_2-1/0 were synthesized by changing the content of $InCI_3$ and Na_2SnO_3. For In-SnO_2-1/1-150, the reaction temperature was 150°C and the content of $InCI_3$ and Na_2SnO_3 was 1:1. Other processes were in line with the fabrication of In-SnO_2-1/1. To prepare the In-SnO_2-1/1-12 and In-SnO_2-1/1-36, the reaction time was 12 and 36 h, respectively. Other parameters remained unchanged. These samples were ready for using after grinding.

Characterization:

The X-ray diffraction (XRD) patterns of catalysts were recorded on an X-ray

diffractometer (D/max 2550) with Cu Kα radiation at a scan rate of 10° min^{-1} from 10° to 90°. The Raman spectra were tested by a Raman spectrometer (LabRAM HR apparatus) with a test range from 0 to 2000 cm^{-1}. For X-ray photoelectron spectroscopy (XPS), a Thermo Fisher Escalab 250Xi XPS instrument with Al Kα as emission source was applied. The spectra were calibrated with the position of C 1s peak (284.8 eV). Electron paramagnetic resonance (EPR) experiments of sample were performed on JES-FA300 under normal conditions. Contact angle measurements of sample were performed on DSA-XROLL. And the FEI TECNAI G2 F20 transmission electron microscope (TEM) was used to observe the morphology of catalysts and analyze their internal structure.

Electrochemical measurements:

To prepare catalyst ink, 6 mg freshly prepared sample and 2 mg acetylene black were dispersed in 970 μL isopropanol/H_2O (1:3) solution containing 30 μL nafion membrane solution. After continuous ultrasound treatment for 2 h, 40 μL catalyst ink was uniformly dripped on a piece carbon paper in a 0.5 cm×0.5 cm area (catalyst loading of 0.96 mg cm^{-2}). After dried at 60℃, the carbon paper with catalysts was directly used as work electrode. Using an electrochemical workstation (CHI 630E), the electrochemical measurements were carried out in a H-type cell with the three-electrode system and Nafion 117 membrane as a separator. The Ag/AgCl electrode and carbon rod served as reference electrode and counter electrode, respectively. And the 0.5 M $KHCO_3$ aqueous solution (30 mL for each half cell) was used as electrolyte. Linear sweep voltammetry (LSV) curves were recorded at the scanning rate of 5 mV s^{-1} after the continuous Ar/CO_2 (99.99%) bubbling more than 30 min. For constant voltage electrolysis, the CO_2 delivered into cathodic electrolyte kept an average rate of 10 mL min^{-1} during the whole electrolysis process. All voltages were calibrated to potentials relative to reversible hydrogen electrode (RHE) according to the equation: $E_{RHE} = E_{Ag/AgCl}+0.0591\times pH+0.197$ V.

The electrochemical active surface area (ECSA) was estimated from the electrochemical double-layer capacitance (C_{dl}). To eliminate the impact of carbon

paper, the 40 μL prepared catalyst ink without acetylene black was coated on a carbon paper (0.5×0.5 cm^2). In this case, a typically potential window of 0.1 V in non-Faradaic potential range was selected. With the scan rates of 20, 30, 50, 80, 100 and 120 mV s^{-1}, the cyclic voltammetry curves were separately recorded in a single cell applying 0.5 M $KHCO_3$ as electrolyte. Using the Δj ($\Delta j = j_a - j_c$, j_c and j_a respectively represented the cathodic and anodic current densities under the OCP against the scan rate to linearly fit a line, half of the slope was the value of C_{dl}. Assuming the average C_{dl} of metal was 20 μF cm^{-2}, it can be concluded as follows: $ECSA = S \times Rf = S \times C_{dl} / (20\ \mu F\ cm^{-2})$. Here, the Rf was roughness factor; S was the surface area of catalytic electrode (0.25 cm^{-2}). The electrochemical impedance spectroscopy (EIS) was evaluated in a similar electrochemical device of ECSA. The test voltage was set to -0.7 V, while the test frequency was 10^{-2}-10^6 Hz. For flow cell configurations, both the catholyte and anolyte were 1 M KOH. The flow rate of CO_2 was 20 mL min^{-1}, while the flow rate of electrolyte was 10 mL min^{-1}.

Product analysis:

After electrolysis process, the gas products collected by air bags were detected through a gas chromatograph (GC) equipped with a thermal conductivity detector and a flame ionization detector, which could respectively quantify the H_2 and CO. The Ar (99.99%) acted as carrier gas. Before experiment, the GC was calibrated by standards gas (CO and H_2) with different concentrations.

The Faraday efficiency (FE) of different reduction products can be calculated as follows: $FE = c \times V \times n \times F \times Q^{-1}$

Here, c represented the concentration of products; V represented the total volume, which was 600 mL for gas and 30 mL for liquid, respectively; n was the number of transferred electrons, which is 2 for both CO, H_2 and HCOO-; F was the Faraday constant (96485 C mol^{-1}); Q was the total charge passing through the circuit during electrolysis, which can be recorded by electrochemical workstation. Further, the partial current density $j_p = j_{total} \times FE \times S^{-1}$.

Fig. S1 The optical photo of In-SnO_2-1/1.

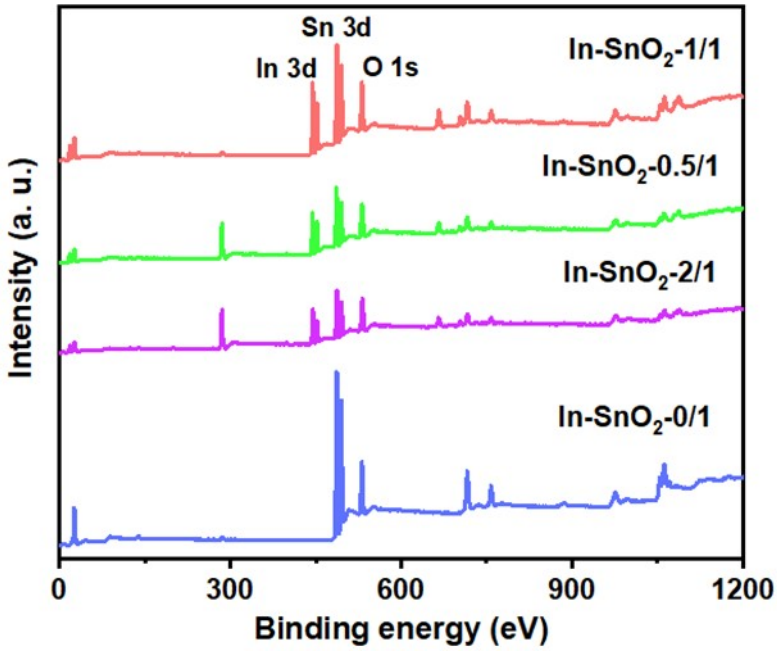

Fig. S2 The XPS survey spectra of In-SnO_2-1/1, In-SnO_2-0.5/1, In-SnO_2-2/1 and In-SnO_2-0/1.

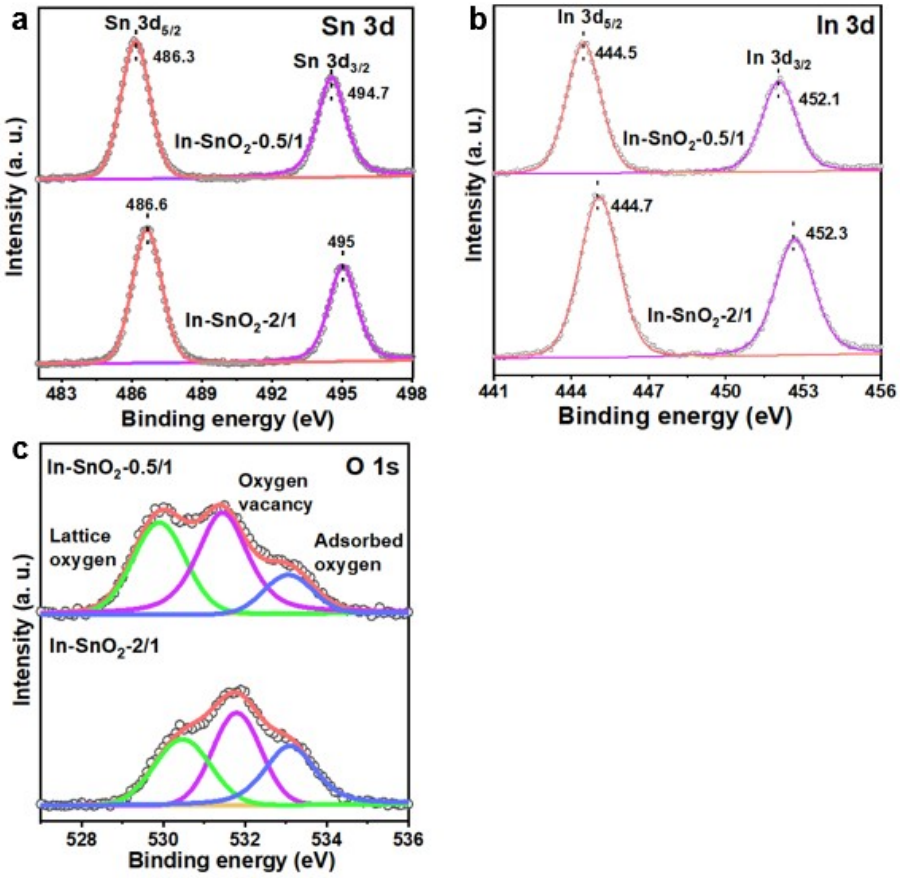

Fig. S3 (a) Sn 3d, (b) In 3d and (c) O 1s spectra of In-SnO_2-0.5/1 and In-SnO_2-2/1.

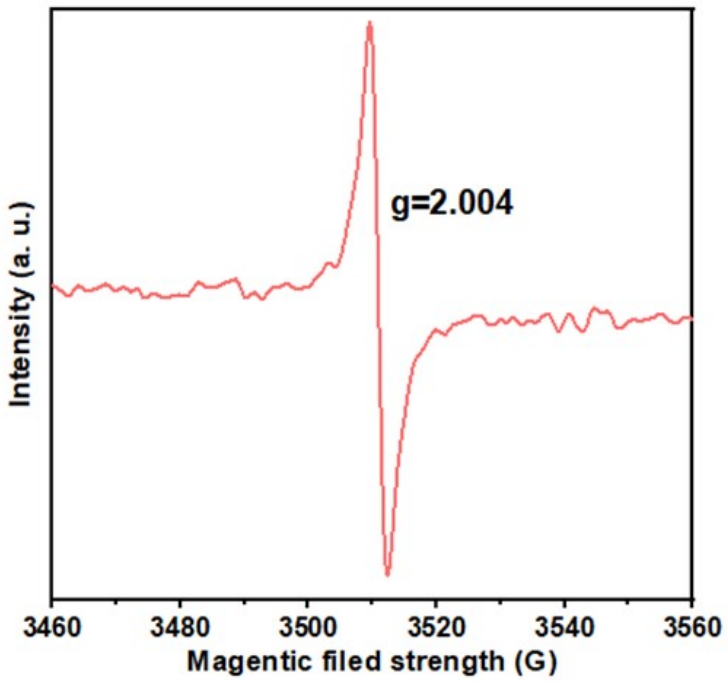

Fig. S4 The EPR of In-SnO_2-1/1.

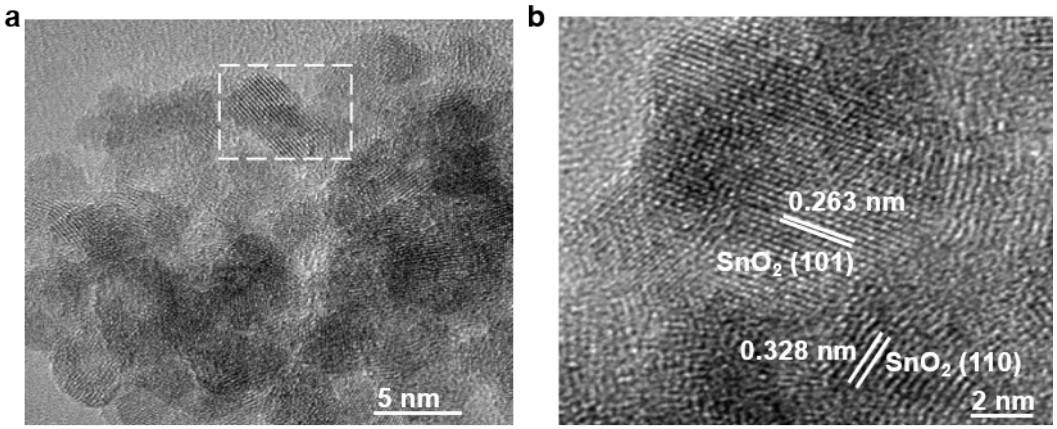

Fig. S5 (a, b) The HRTEM images of In-SnO_2-1/1.

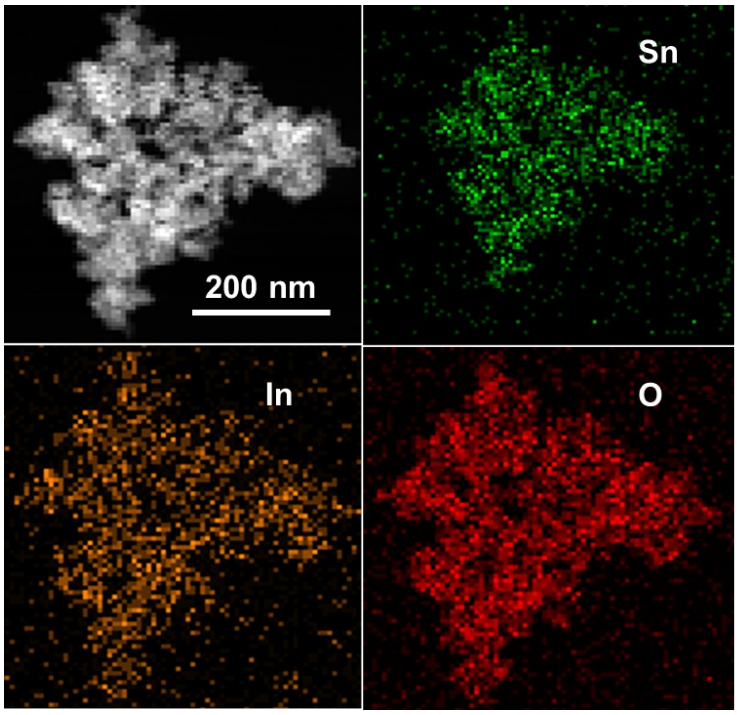

Fig. S6 The EDS elemental mapping images of In-SnO_2-1/1.

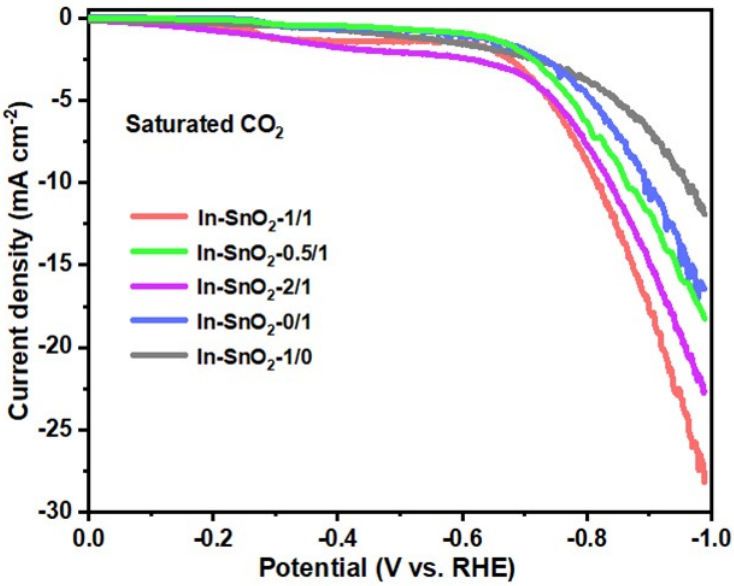

Fig. S7 The LSV curves of different samples under CO_2 atmosphere.

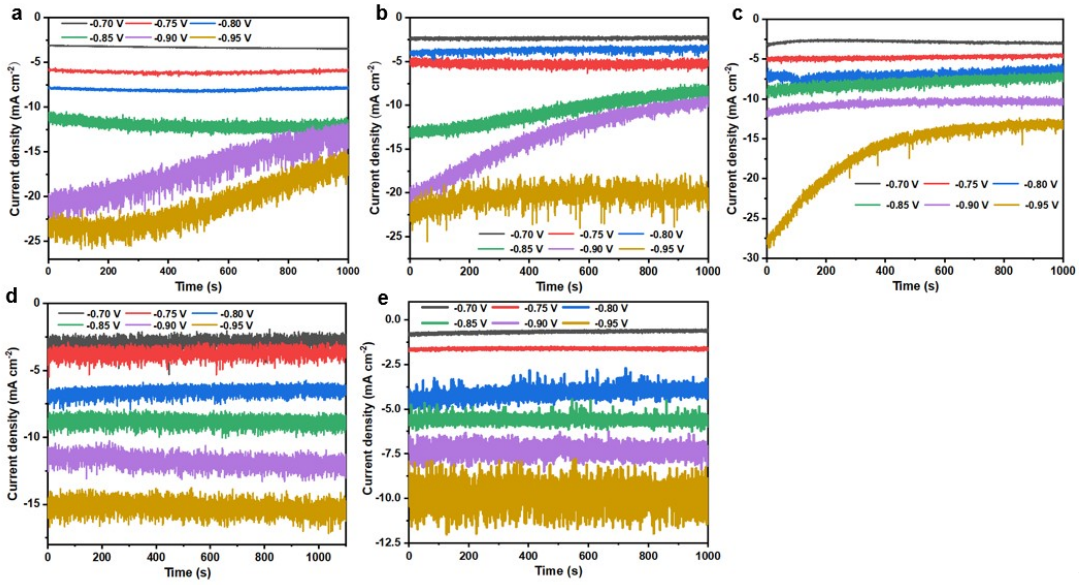

Fig. S8 The i-t curves of (a) In-SnO_2-1/1, (b) In-SnO_2-0.5/1, (c) In-SnO_2-2/1, (d) In-SnO_2-0/1 and (e) In-SnO_2-1/0.

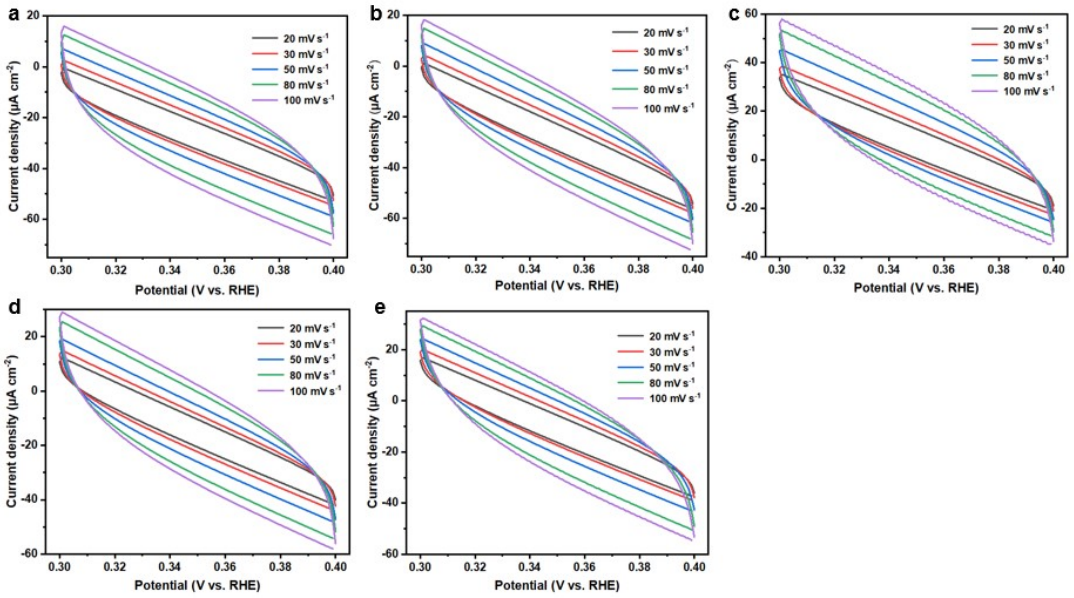

Fig. S9 The CV curves at different scan rates of (a) In-SnO_2-1/1, (b) In-SnO_2-0.5/1, (c) In-SnO_2-2/1, (d) In-SnO_2-0/1 and (e) In-SnO_2-1/0.

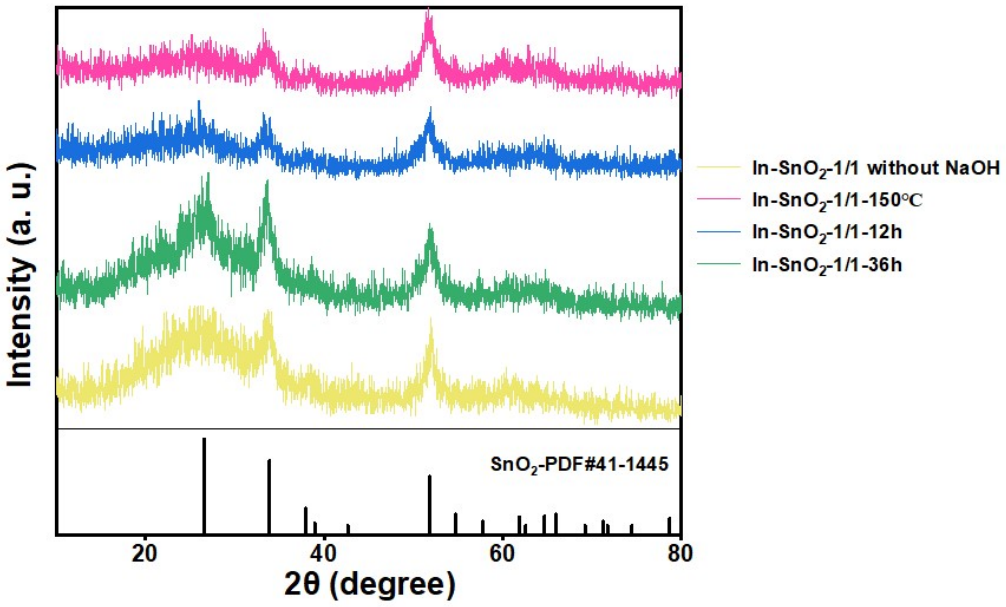

Fig. S10 The XRD patterns of samples under different synthesis conditions.

The XRD patterns of samples with different reaction conditions were displayed in Fig. S10, ESI†. All samples showed identical characteristic peaks for tetragonal rutile-like SnO_2. As the temperature reduced to 150℃, the obtained sample attained the maximum FE_{C1} of 91.08% at -0.85 V, lowering than that of In-SnO_2-1/1 (Fig. S11, ESI†). The pH value of solution was also vital. Sample without NaOH addition displayed a poor selectivity (FE_{C1} < 90%) in all potentials (Fig. S12, ESI†), which was possibly ascribed to the effect of alkaline environment on the conversion processes of Na_2SnO_3 to SnO_2. Besides, when the reaction time was shortened to 12 h or extended to 36 h, both the FE and the partial current density for C_1 products significantly decreased (Fig. S13, ESI†).

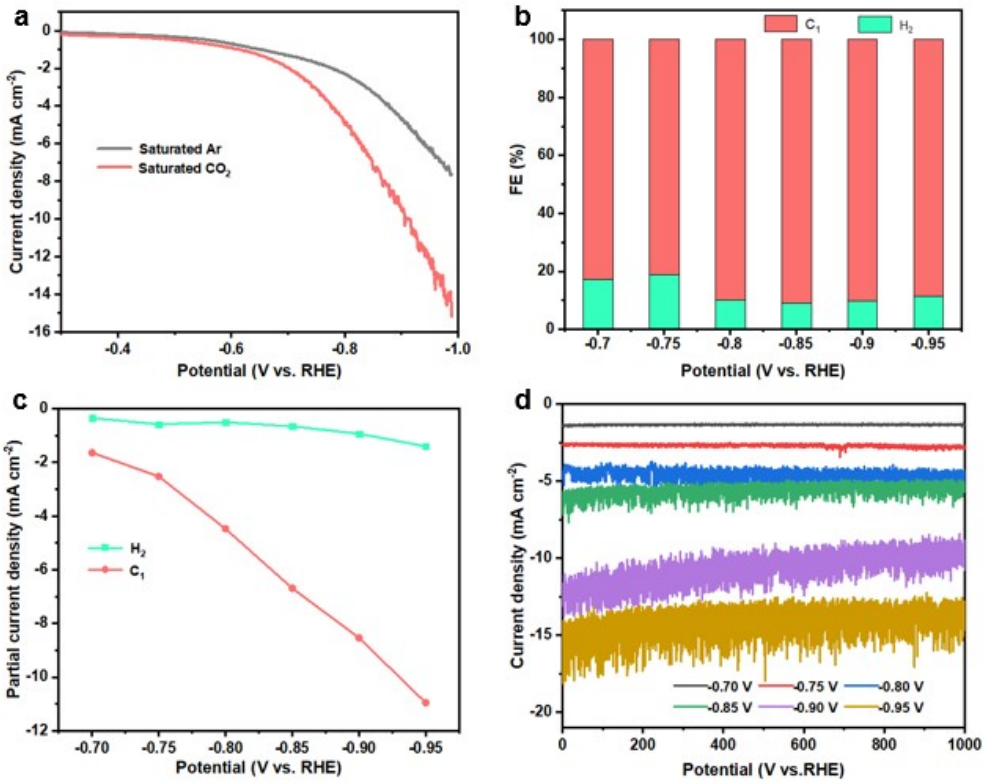

Fig. S11 (a) The LSV, (b) FE, (c) partial current density and (d) i-t curves of In-SnO_2-1/1-150℃.

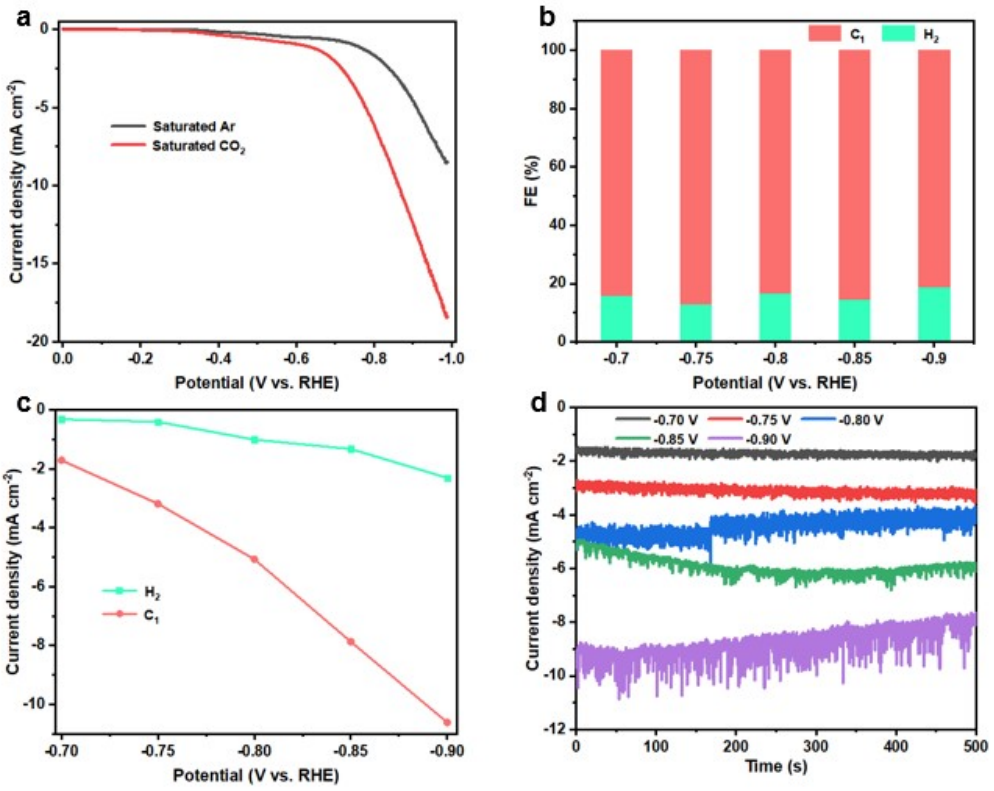

Fig. S12 (a) The LSV, (b) FE, (c) partial current density and (d) i-t curves of In-SnO_2-1/1 without NaOH addition.

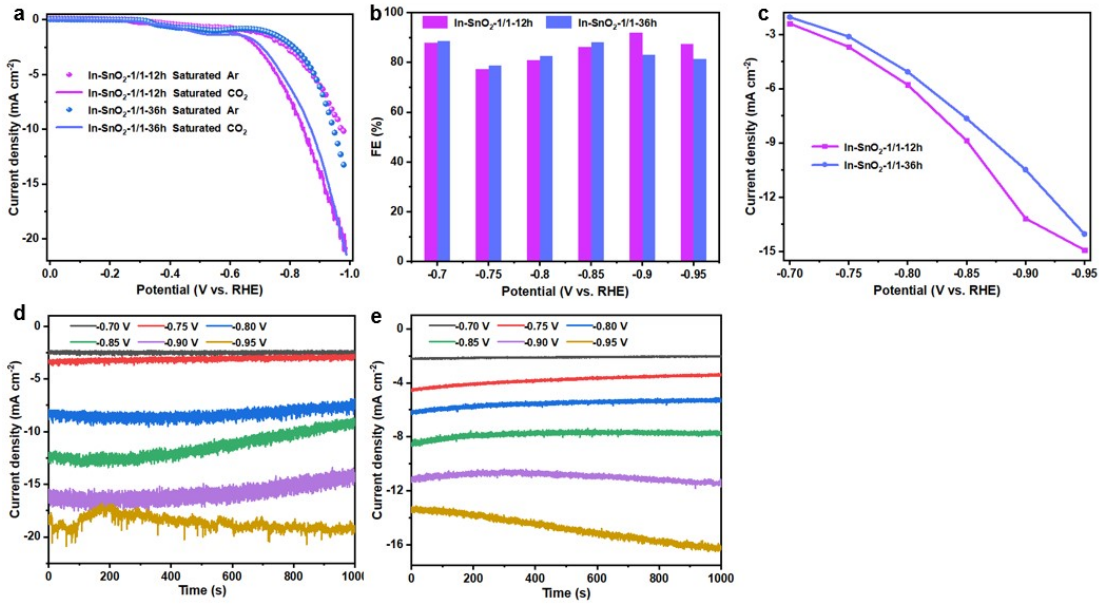

Fig. S13 (a) The LSV, (b) FE and (c) partial current density curves of different samples. The i-t curves of (d) In-SnO_2-1/1-12 h and (e) In-SnO_2-1/1-36 h.

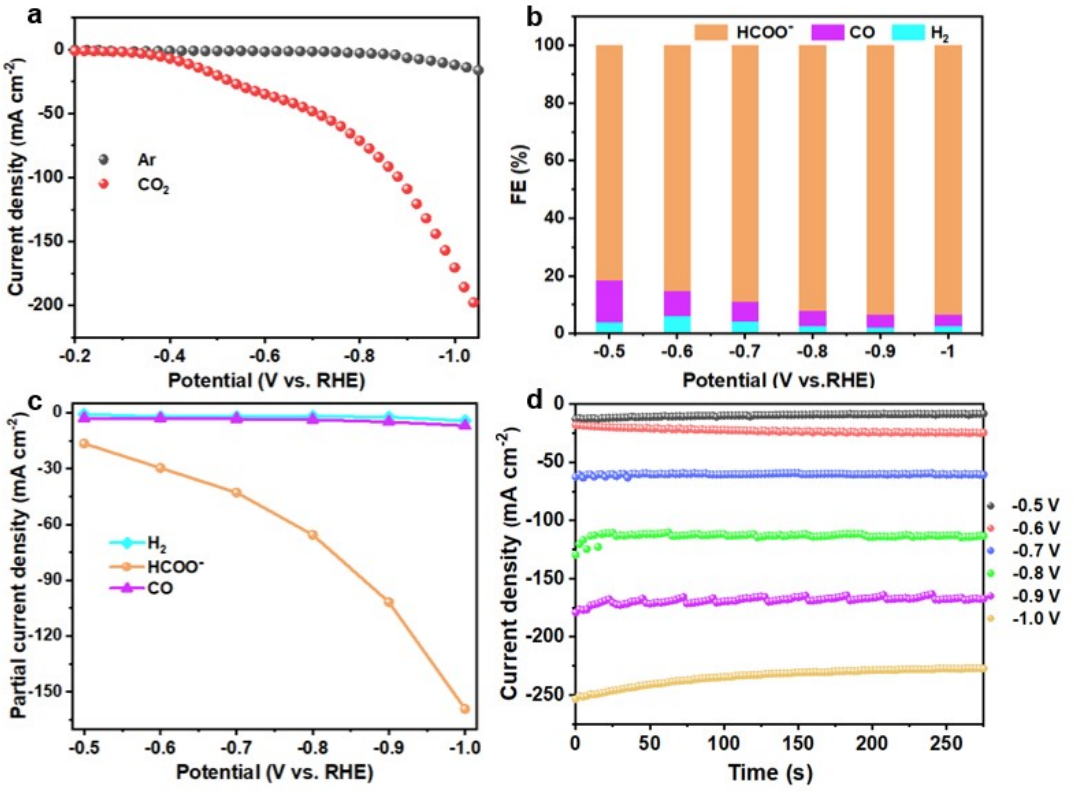

Fig. S14 (a) The LSV curves, (b) FE, (c) partial current density of reduction products and (d) i-t curves at different potentials for In-SnO_2-1/1 in flow cells.

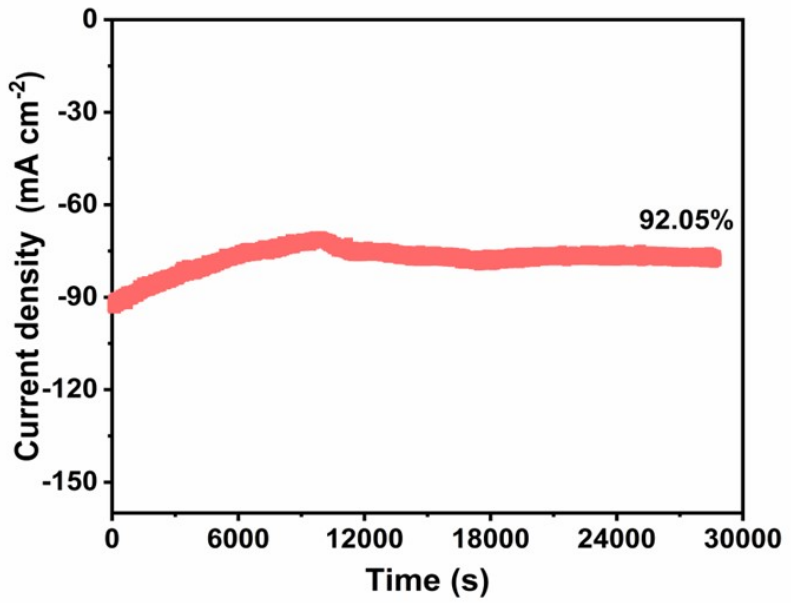

Fig. S15 The stability test of In-SnO_2-1/1 at -0.8 V in flow cell.

Table S1 The product distribution ($HCOO^-$ and CO) of In-SnO_2-1/1 at different potentials in H-type electrolyzers

Potential (V vs. RHE)	FE_{HCOO-} (%)	FE_{CO} (%)
-0.70	63.98	28.85
-0.75	73.32	23.14
-0.80	74.06	21.26
-0.85	72.45	21.19
-0.90	69.31	21.16
-0.95	70.19	18.63

Table S2 The preparation and performance comparison of various electrocatalysts for CO_2RR to C_1.

Catalysts	Main raw materials	Methods	Reaction conditions	Electrolytes	FE (%)	J_{C1} (mA cm^{-2})	Notes	Refs.
In-SnO_2-1	Na_2SnO_3, $InCI_3$, NaOH, deionized water	Hydrothermal	180°C, 24 h	0.5 M $KHCO_3$	96.46% (-0.75 V)	-20.12 (-0.95 V)		This work
V_O-rich N-SnO_2 NS	$SnCl_2{\cdot}2H_2O$, ethylenediamine, ammonia	Hydrothermal, ammonification reaction	180°C, 24 h; 550°C, 1 h	0.1 M $KHCO_3$	99.05% (-1.1 V)	-16.75 (-1.2 V)	High temperature	1
Pd-timtmb^{Me}	1,3,5-tris(bromomethyl)-2,4,6-trimethylbenzene, 1-methylimidazole, 1-Isopropylimidazole, acetone, palladium foil	Organic transformation, calcination, in situ transformation	Room temperature, 6 h; 600°C, 8 h; room temperature, 12 h	0.5 M $KHCO_3$	86% (-0.57 V)	-5.86 (-0.87 V)	High temperature and multi-procedure synthesis	2
WIT SnO_2 nanofibers	$SnCl_2{\cdot}2H_2O$, PVP, DMF, ethanol	Electrospinning, calcination	Room temperature, 15 kV; 500°C, 2 h	0.1 M $KHCO_3$	93% (-0.99 V)	-10.8 (-1.29 V)	High temperature	3
Sn NCs:S	1,2-BDT, $SnCl_4$	Self-assembly	Ice bath, 17 h	0.5 M $KHCO_3$	97% (-0.97 V)	-30.56 (-0.97 V)	High toxicity	4
P2-GaIn CNPs/PDDA-MWCNTs	P2-GaIn crystals, acetone, MWCNTs, borate buffer, PDDA	Electrostatic self-assembly	Room temperature, 30 min	0.1 M $KHCO_3$	84.4% (-1.0 V)	-8.2 (-1.0 V)	Poor CO_2RR performance	5
Sn/SnO_2-2h	$SnCl_2$ $2H_2O$, PTA, TMA, deionized water	Hydrothermal, thermal reduction	180°C, 24 h; 400°C, 2 h	0.5 M $KHCO_3$	92.5% (-1.0 V)	-27.02 (-1.0 V)	High temperature	6

In_2O_3-0	In_2O_3 power	Magnetron sputtering	Room temperature, 120 W, oxygen partial pressure of 0	0. 1M $KHCO_3$	83% (-0.85 V)	-2.86 (-0.85 V)	Poor CO_2RR performance	7
In/In oxide heterostructures	TPA, DMF, $In(NO3)_3$ xH_2O	Oil bath, thermal reduction	120℃, 20 min; 400℃, 4 h;	0.5 M $KHCO_3$	98.45% (-0.7 V)	-45.47 (-1.1 V)	High temperature	8
SnO_2⊃NC@EEG	PVP, 2MeIm, DMF, EEG suspension,	Electrochemical exfoliation, hydrothermal, pyrolysis	Room temperature, 2 h; 160℃, 12 h; 500℃, 3 h	0.1 M $KHCO_3$	93.2% (-1.2 V)	-11.93 (-1.2 V)	High temperature and high overpotentials	9
P-SnO_2-0	Sn, Se, choline chloride, $N_2H_4·H_2O$,	Hydrothermal, calcination	150℃, 24 h; 800℃, 0 min	0.1 M $KHCO_3$	94.5% (-1.06 V)	-11.5 (-1.06 V)	High temperature and small current density of C_1	10
$CuSn_{0.175}$ NPs on NG	Graphene oxide, DMF, $Cu(NO_3)_2·2H_2O$, $SnCl_4$, dicyandiamide	Hydrothermal, pyrolysis	200℃, 4 h; 900℃, 2 h	0.5 M $KHCO_3$	93% (-1.0 V)	-13.02 (-1.0 V)	High temperature and small current density of C_1	11
D-NR	$Bi(NO_3)_3·5H_2O$, $C_5H_{10}NNaS_2·3H_2O$	Hydrothermal	140℃, 10 h;	0.5 M $KHCO_3$	82% (-1.0 V)	-11 (-1.2 V)	Poor CO_2RR performance	12
Cu_1Ni_2@ N-MWCNT	$Cu(NO_3)_2·3H_2O$, MWCNTs $Ni(NO_3)2·6H_2O$, citric acid Monohydrate	Hydrothermal, calcination	80℃, 12 h; 200℃, 1 h	0.5 M $KHCO_3$	90% (-0.53 V)	-5.4 (-0.53 V)	High temperature and small current density of C_1	13
Oct-{111} NPs	$SnCl_4$ $5H_2O$, HCl, PVP ethanol, distilled water	Hydrothermal	200℃, 12h	0.5 M $NaHCO_3$	96.02% (-1.0 V)	-10.08 (-1.0 V)	High temperature and small current density of C_1	14

Table S3 The product distribution ($HCOO^-$ and CO) of In-SnO_2-1/1 at different potentials in flow cells

Potential (V vs. RHE)	FE_{HCOO-}	FE_{CO}
-0.5	81.71	14.44
-0.6	85.27	8.81
-0.7	88.93	6.93
-0.8	92.17	5.21
-0.9	93.38	4.51
-1.0	93.4	4.06

References

[1] Z. J. Li, A. Cao, Q. Zheng, Y. Y. Fu, T. T. Wang, K. T. Arul, J. L. Chen, B. Yang, N. M. Adli, L. C. Lei, C. L. Dong, J. P. Xiao, G. Wu and Y. Hou, *Adv. Mater.*, 2021, **33**, 2005113.

[2] Z. Cao, J. Derrick, J. Xu, R. Gao, M. Gong, E. Nichols, P. Smith, X. W. Liu, X. D. Wen, C. Coperet and C. Chang, *Angew. Chem. Int. Ed.*, 2018, **57**, 4981.

[3] L. Fan, Z. Xia, M. J. Xu, Y. Y. Lu and Z. J. Li, *Adv. Funct. Mater.*, 2018, **28**, 1706289.

[4] X. Wang, F. L. Li, W. J. Yin, Y. B. Si, M. Miao, X. M. Wang and Y. Z. Fu, *Appl. Catal. B-Environ.*, 2022, **304**, 120936.

[5] X. Wang, X. L. Wang, J. Lv, Z. Wu, J. X. Zhang, D. D. Hu, C. Z. Xue, D. S. Li, X. Zhu and T. Wu, *Chem. Eng. J.*, 2021, **422**, 130045.

[6] X. Y. Cao, B. R. Wulan, B. H. Zhang, D. X. Tan and J. T. Zhang, *J. Mater. Chem. A*, 2021, **9**, 14741.

[7] X. Y. Du, Y. Y. Qin, B. Gao, K. Wang, D. Li, Y. H. Li, S. J. Ding, Z. X. Song, Y. Q. Su and C. H. Xiao, *Appl. Surf. Sci.*, 2021, **563**, 150405.

[8] W. F. Yang, Y. Zhao, S. Chen, W. H. Ren, X. J. Chen, C. Jia, Z. Su, Y. Wang and C. Zhao, *Inorg. Chem.*, 2020, **59**, 12437.

[9] Y. Y. Fu, T. T. Wang, W. Z. Zheng, C. J. Lei, B. Yang, J. Chen, Z. J. Li, L. C. Lei, C. Yuan and Y. Hou, *ACS Appl. Mater. Interfaces*, 2020, **12**, 16178.

[10] S. Zhang, M. Sun, K. Y. Wang, L. Cheng, S. Zhang and C. Wang, *ACS Sustainable Chem. Eng.*, 2021, **9**, 2358.

[11] W. Xiong, J. Yang, L. Shuai, Y. Hou, M. Qiu, X. Y. Li and M. K. H. Leung, *ChemElectroChem*, 2019, **6**, 1.

[12] Y. T. Wang, L. Cheng, J. Z. Liu, C. Q. Xiao, B. Zhang, Q. H. Xiong, T. Zhang, Z. L. Jiang, H. Jiang, Y. H. Zhu, Y. H. Li and C. Z. Li, *ChemElectroChem*, 2020, **7**, 2864.

[13] M. C. Wang, Z. Z. Cai, B. K. Zhang, K. W. Yang, T. Y. Shou, M. T. Bernards, P. F. Xie, Y. He and Y. Shi, *Energy Fuels*, 2022, **36**, 5833.

[14] M. L. Fang, Z. P. Zheng, J. Y. Chen, Q. Chen, D. Y. Liu, B. B. Xu, J. Y. Wu, Q. Kuang and Z. X. Xie, *Sustainable Energy Fuels*, 2020, **4**, 600.